The Astrophysical Journal Letters, 774:L21 (6pp), 2013 September 10 doi:10.1088/2041-8205/774/2/L21

OPTICAL PROPER MOTION MEASUREMENTS OF THE M87 JET: NEW RESULTS FROM THE *HUBBLE SPACE TELESCOPE*

Eileen T. Meyer[1], W. B. Sparks[1], J. A. Biretta[1], Jay Anderson[1], Sangmo Tony Sohn[1], Roeland P. van der Marel[1], Colin Norman[1,2], and Masanori Nakamura[3]
[1] Space Telescope Science Institute, 3700 San Martin Drive, Baltimore, MD 21218, USA; meyer@stsci.edu
[2] Department of Physics and Astronomy, Johns Hopkins University, Baltimore, MD 21218, USA
[3] Institute of Astronomy and Astrophysics, Academia Sinica, P.O. Box 23-141, Taipei 10617, Taiwan
Received 2013 June 10; accepted 2013 July 14; published 2013 August 22

ABSTRACT

We report new results from a *Hubble Space Telescope* archival program to study proper motions in the optical jet of the nearby radio galaxy M87. Using over 13 yr of archival imaging, we reach accuracies below 0.1c in measuring the apparent velocities of individual knots in the jet. We confirm previous findings of speeds up to 4.5c in the inner 6″ of the jet, and report new speeds for optical components in the outer part of the jet. We find evidence of significant motion transverse to the jet axis on the order of 0.6c in the inner jet features, and superluminal velocities parallel and transverse to the jet in the outer knot components, with an apparent ordering of velocity vectors possibly consistent with a helical jet pattern. Previous results suggested a global deceleration over the length of the jet in the form of decreasing maximum speeds of knot components from HST-1 outward, but our results suggest that superluminal speeds persist out to knot C, with large differentials in very nearby features all along the jet. We find significant apparent accelerations in directions parallel and transverse to the jet axis, along with evidence for stationary features in knots D, E, and I. These results are expected to place important constraints on detailed models of kiloparsec-scale relativistic jets.

Key words: astrometry – galaxies: active – galaxies: individual (M87) – galaxies: jets

Online-only material: color figures, animations

1. INTRODUCTION

The nearby radio galaxy M87, a giant elliptical near the center of the Virgo cluster, hosts a striking optical jet extending 20″ to the northwest of a blazar-like core, as first observed by Curtis (1918). This source has been extensively observed in the radio, infrared, optical, and X-rays (e.g., Owen et al. 1989; Sparks et al. 1996; Perlman et al. 2001; Walker et al. 2008; Marshall et al. 2002; Perlman & Wilson 2005). At a distance of only 16.7 Mpc (81 pc arcsec^{-1}; Blakeslee et al. 2009), structures on the order of parsecs can easily be resolved using high-resolution instruments such as the *Hubble Space Telescope* (*HST*). The bright knots of emission spread along the 1.6 kpc (projected) jet in optical and X-ray imaging correspond to features seen in the radio, with a spectrum consistent with synchrotron emission (Marshall et al. 2002).

Proper motion studies are integral to our understanding of relativistic jets, as apparent velocities ($\beta_{\rm app} = v/c$) give lower limits to the bulk Lorentz factor and upper limits on the angle to the line of sight, as well as detailed kinematics for comparison to theoretical jet models. Almost all proper motion studies of jetted active galactic nucleus have used very long baseline interferometry (VLBI), and in the case of M87 have revealed sub-relativistic speeds in small components within a parsec of the core (Reid et al. 1989; Junor & Biretta 1995; Kovalev et al. 2007). *Superluminal* motions have also been measured in the kiloparsec-scale jet with both the Very Large Array (Biretta et al. 1995, hereafter B95), and in the optical with *HST* (Biretta et al. 1999, hereafter B99). The latter study measured only the inner 6″ of the jet, and suffered from rather larger errors (on the order of 0.3–1c). However, in comparison to radio measurements, the optical jet emission traces higher energy electron populations more closely associated with the sites of acceleration, leading to more compact features which can be precisely measured.

In this Letter, we present the initial results of an archival study of proper motions in the M87 jet with *HST*. The aim of this work is to leverage 13.25 yr of *Hubble* observations of M87 to vastly improve on previous measurements of apparent velocities in the jet, reaching accuracies better than 0.1c in order to map the detailed velocity field of the jet as it propagates from the core, including transverse motions and accelerations.

2. OBSERVATIONS

2.1. Hubble Archival Data

Because jet components are known to differ in size, intensity, and apparent location with wavelength, we used archival images only in a single filter, F814W (wide *I* band), which gives the longest possible baseline of 13.25 yr and a dense sampling in time. The total data set is comprised of nearly all the Advanced Camera for Surveys High Resolution Channel (ACS/HRC) and Wide Field Channel (ACS/WFC) archival images as well as those from WFPC2 (PC chip) in this filter. For ACS/HRC, we used 30 (48–50 s) exposures spanning 2002 November to 2006 November. For ACS/WFC, we used 217 dithered exposures (all 360 s) taken in 2006. For WFPC2, we used 161 exposures of 160–600 s, spanning 1995–2008; several shorter exposures of 30–40 s were not used due to poor signal-to-noise ratio.

2.2. Astrometry Methods

The general method we have used is similar to that used (and described in detail) in Anderson & van der Marel (2010) and Sohn et al. (2012). The reference frame is based on the positions of hundreds of bright globular clusters associated with the host galaxy which are easily detected in the ACS/WFC images and are effectively stationary to proper motions over the time of this study. As cluster positions do not change

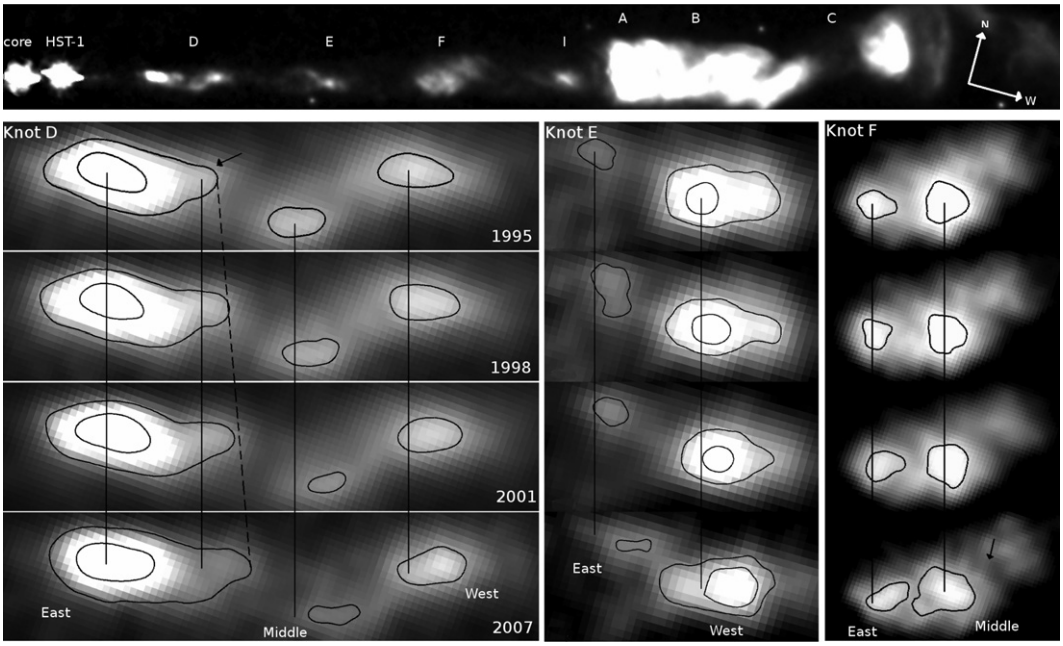

Figure 1. Top figure: the entire jet, from a stack of ACS/WFC F606W images taken in 2006 with galaxy subtracted. All other images are taken from stacks of WFPC2 exposures in the F814W filter. Lower left: within knot D, D-East appears to be nearly stationary, while D-Middle appears to move at $4.27 \pm 0.30c$ along the jet. D-West is the only knot to show a strong deceleration in the jet direction, apparent when comparing the 2001 and 2007 epochs. The new component noted with an arrow appears to move at $\sim 2.4c$ (vertical lines in all figures are to guide the eye). Lower middle: knot E appears complex, with a new extension to the east of the main knot (E-West) appearing in 2008. Lower right: knot F shows evidence of complex, even clumpy structure. F-Middle is moving at $0.36 \pm 0.14c$ and appears to be fading over time. Animations of the entire jet and the components highlighted in the subfigures (Figures 1 and 3) are available online. In all cases, the images are scaled linearly with a maximum (white color) at 2000 total electron units, except in the knot A/B animation which is scaled to a maximum at 8000 electron units (equivalent to 600 s ACS exposure).

(Animations of this figure are available in the online journal.)

with filter, the reference frame was built using 56 (500 s) ACS/WFC exposures of the field in the F606W filter, which has slightly better resolution than F814W. The reference frame was created by first detecting the positions of the globular clusters in each flat-fielded, Charge Transfer Efficiency (CTE)-corrected ACS/WFC image[4] using a point-spread function peak-fitting routine, then applying the standard (filter-specific) geometric correction to those positions, and then finding the best linear transformation for each image which matches the positions in the individual (geometrically corrected) frames to a master reference frame. This last step is done by a routine similar to MultiDrizzle, but better optimized for astrometry. The process of finding transformations for all frames is iterated so that the master reference frame (super-sampled to a pixel scale of $0\farcs025$ pixel^{-1}) effectively gives the average position of each reference source in a geometrically corrected frame.

The final reference system consists of positions and magnitudes for 1378 globular clusters within $\sim 100''$ of the M87 core position. Among all clusters, the median one-dimensional rms residual relative to the mean position was 0.05 (reference frame) pixels (1.25 mas), corresponding to a systematic astrometric accuracy ($\times 1/\sqrt{56}$) of 0.17 mas; over the 13.25 yr baseline this is equivalent to $0.003c$.

Astrometric solutions were then found for all the ACS/HRC, ACS/WFC, and WFPC2 images in F814W, except that the linear transformation solution between the individual (corrected) images and the reference frame was found once rather than iterated. Typical numbers of globular clusters used to match the frames were $\sim$200–500 for ACS/WFC, $\sim$15–30 for WFPC2 images, and $\sim$15–25 for ACS/HRC; corresponding systematic errors were $\sim$0.006, $\sim$0.03, and $\sim$0.05 pixels, or $0.003c$, $0.015c$, $0.025c$ over 13.25 yr, respectively.

2.3. Measuring the Jet Knot Positions

Because of the difficulty in measuring the diffuse/complex knot structures particularly in the noisy HRC images and shorter WFPC2 images, we chose to first identify the peaks of interest using stacked images. The image stacks include the 2006 ACS/WFC stack, four WFPC2 stacks (epochs 1995–1996, 1998–1999, 2001, and 2007–2008), and three stacks of ACS/HRC exposures (2002 November–2003 November, 2004 July–2005 September, 2005 November–2006 November). The host galaxy was modeled using the ACS/WFC stacked image with the IRAF/STSDAS tasks *ellipse* and *bmodel* and then subtracted. Seven jet regions were cut out from these images, corresponding to knots HST-1, D, E, F, I, A+B, and C (see Figure 1).

A two-dimensional continuous functional representation of the image cutouts was then created using the Cosine Transform function (*FourierDCT*) in *Mathematica*, which allowed us to find prominent peaks, as well as contours of constant flux level around those peaks. In general, the number of interesting peaks was chosen by hand, and the contour line levels were at 50% of the flux of the peak, after a "background" level was subtracted, the latter estimated as the minimum flux level between the particular peak and the next nearest peak. The positions defining the contour were "reverse-transformed" from master frame coordinates into each distorted, galaxy-subtracted image so that an intensity-weighted centroid position from the pixels within the contour could be calculated. These final positions were then transformed back into the common reference frame, so that

[4] ACS/HRC and WFPC2 data were not used due to inferior in signal-to-noise quality to the longer ACS/WFC images, and to avoid complications of combining different instruments.

Table 1
Linear and Quadratic Fits to Individual Components

Knot	Subknot	Distance[a]		Linear Fit		Quadratic Fit				Speed[d]	
		(″)	(kpc)	μ_x (mas yr^{-1})	μ_y (mas yr^{-1})	μ_x (mas yr^{-1})	ξ_x (mas yr^{-2})	μ_y (mas yr^{-1})	ξ_y (mas yr^{-2})	β_x (c)	β_y (c)
D	East	2.77	0.224	1.1 ± 0.2	-0.2 ± 0.1					0.28 ± 0.05	-0.05 ± 0.03
	Middle[b]	3.61	0.292	16.2 ± 1.1	-0.7 ± 0.1			-1.3 ± 0.2	-0.2 ± 0.1	4.27 ± 0.30	-0.35 ± 0.05
	West	3.97	0.321	5.7 ± 0.5	-2.2 ± 0.2	3.9 ± 0.5	-0.80 ± 0.2			1.03 ± 0.14	-0.59 ± 0.05
E	East	5.86	0.473	9.6 ± 1.2	-1.8 ± 0.3					2.52 ± 0.32	-0.48 ± 0.08
	West	6.21	0.502	7.2 ± 0.5	0.0 ± 0.2					1.91 ± 0.14	-0.01 ± 0.05
F	East	8.23	0.666	7.0 ± 0.9	-1.3 ± 0.4					1.85 ± 0.24	-0.35 ± 0.12
	Middle	8.68	0.702	1.4 ± 0.5	0.7 ± 0.5			2.2 ± 0.5	0.6 ± 0.2	0.36 ± 0.14	0.58 ± 0.14
I		11.01	0.890	-0.9 ± 0.4	-0.1 ± 0.2					-0.23 ± 0.12	-0.02 ± 0.07
A	A1	12.28	0.993	5.0 ± 0.4	2.4 ± 0.3			3.1 ± 0.3	0.3 ± 0.1	1.32 ± 0.12	0.82 ± 0.09
	A2	12.60	1.019	1.2 ± 0.2	1.9 ± 0.6					0.31 ± 0.06	0.50 ± 0.16
B	B1	12.88	1.041	5.2 ± 0.6	-0.6 ± 0.9			2.0 ± 1.0	1.1 ± 0.3	1.37 ± 0.16	0.53 ± 0.26
	B2	13.16	1.064	1.6 ± 0.3	-1.4 ± 0.2			-0.8 ± 0.3	0.2 ± 0.1	0.42 ± 0.07	-0.22 ± 0.08
	B3	13.74	1.110	1.3 ± 0.2	1.2 ± 0.1	1.9 ± 0.2	0.3 ± 0.1	1.6 ± 0.2	0.2 ± 0.1	0.49 ± 0.05	0.42 ± 0.04
	B4	14.29	1.155	6.3 ± 0.4	-3.3 ± 0.5			-1.7 ± 0.3	0.7 ± 0.1	1.66 ± 0.11	-0.45 ± 0.08
	B5-s	15.18	1.227	7.2 ± 0.3	2.8 ± 0.3			1.8 ± 0.3	-0.4 ± 0.1	1.90 ± 0.09	0.48 ± 0.07
	B5-n	15.18	1.227	8.2 ± 1.3	4.9 ± 1.2					2.16 ± 0.35	1.30 ± 0.31
C	C1	17.48	1.413	3.3 ± 0.4	-0.6 ± 0.3			0.3 ± 0.3	0.4 ± 0.1	0.86 ± 0.10	0.07 ± 0.08
	C2	17.83	1.441	2.4 ± 0.3	-1.7 ± 1.2	1.5 ± 0.2	-0.4 ± 0.1	-5.6 ± 0.9	-1.6 ± 0.3	0.41 ± 0.06	-1.47 ± 0.23
	C3	17.90	1.447	2.2 ± 0.5	0.7 ± 0.6			-1.7 ± 0.3	-1.0 ± 0.1	0.57 ± 0.13	-0.45 ± 0.07
	C2+C3	17.83	1.441	3.2 ± 0.4	-2.1 ± 0.3					0.83 ± 0.12	-0.54 ± 0.08
GC[c]	(single)			0.0 ± 0.22	0.31 ± 0.15					0.00 ± 0.06	0.08 ± 0.04
	(mean)			0.0 ± 0.06	0.00 ± 0.06					0.00 ± 0.02	0.00 ± 0.02

Notes. No HRC data was used for knots D-Middle, F, A, B, and C due to poor signal-to-noise.
[a] Distance from the core as measured in the 1995 epoch WFPC2 stacked image.
[b] No data after 2007 used in fit due to feature fading.
[c] Examples of globular cluster (GC) fits, including a single faint GC near knot A and the ensemble average.
[d] Quadratic fit given when preferred at >95% level, where β values in those cases correspond to the mean time 2004.06.

each peak of interest was measured in every exposure, resulting in hundreds of position measurements spread over the 13 yr baseline.

To measure the apparent motion of the jet components over time, we define the x-direction as the line from the core through the center of knot I (position angle of 290°), with y-direction perpendicular. Data were binned into 26 time bins (depicted in Figure 2), and a linear model was fit using standard weighted least squares. The weights were taken to be the inverse of the variance for each time bin, as measured from the 10 nearby globular cluster reference sources (discussed below). For each feature and in each direction, we also attempted to fit the data with a quadratic to look for accelerations. When the analysis of variance favored the quadratic over the linear model at a 95% level or greater, the quadratic fit is noted in Table 1 along with the linear fit. The apparent speed ($\beta_{\rm app}$) in each direction in units of c is also given; where the quadratic fit is favored $\beta_{\rm app}$ corresponds to the speed at the mean date of 2004.06.

2.4. The Globular Clusters as Controls

The method was tested using 10 globular clusters near to the jet, each of which was measured as described above, with contour levels drawn at 50% of the peak intensity. Each set of cluster positions was binned into the 26 time bins spread between 1995 and 2008, and for each bin the mean position for all 10 clusters was subtracted from the positions so that the variance in the estimates could be measured from all clusters as a function of epoch for use in the weighted linear least-squares fit. The measured variance was essentially constant across all epochs at ∼0.1 reference pixels. Linear fits to the x- and y-direction positions versus time in all cases were consistent with a

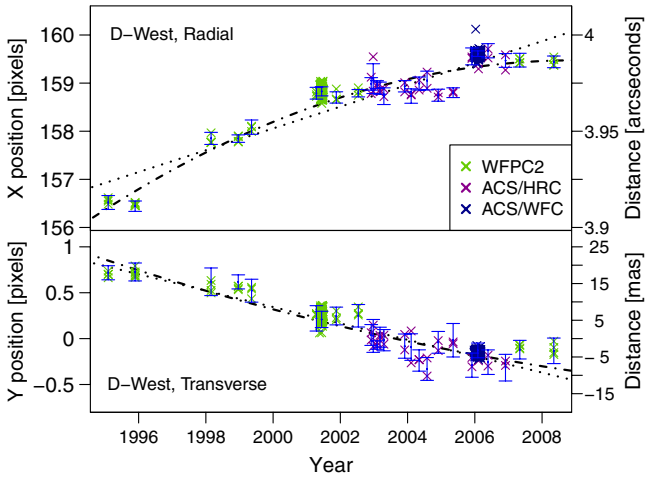

Figure 2. Upper panel: distance from the core vs. time for knot D-West. The blue points show the mean values for each time bin with errors estimated from nearby globular clusters. This knot shows a remarkable deceleration over time, from an initial speed of ∼2.7c in 1996 to near zero by the end of the time series. Lower panel: the rapid transverse velocity of knot D-West is apparent in this plot of y-coordinate vs. time, corresponding to −0.59c.
(A color version of this figure is available in the online journal.)

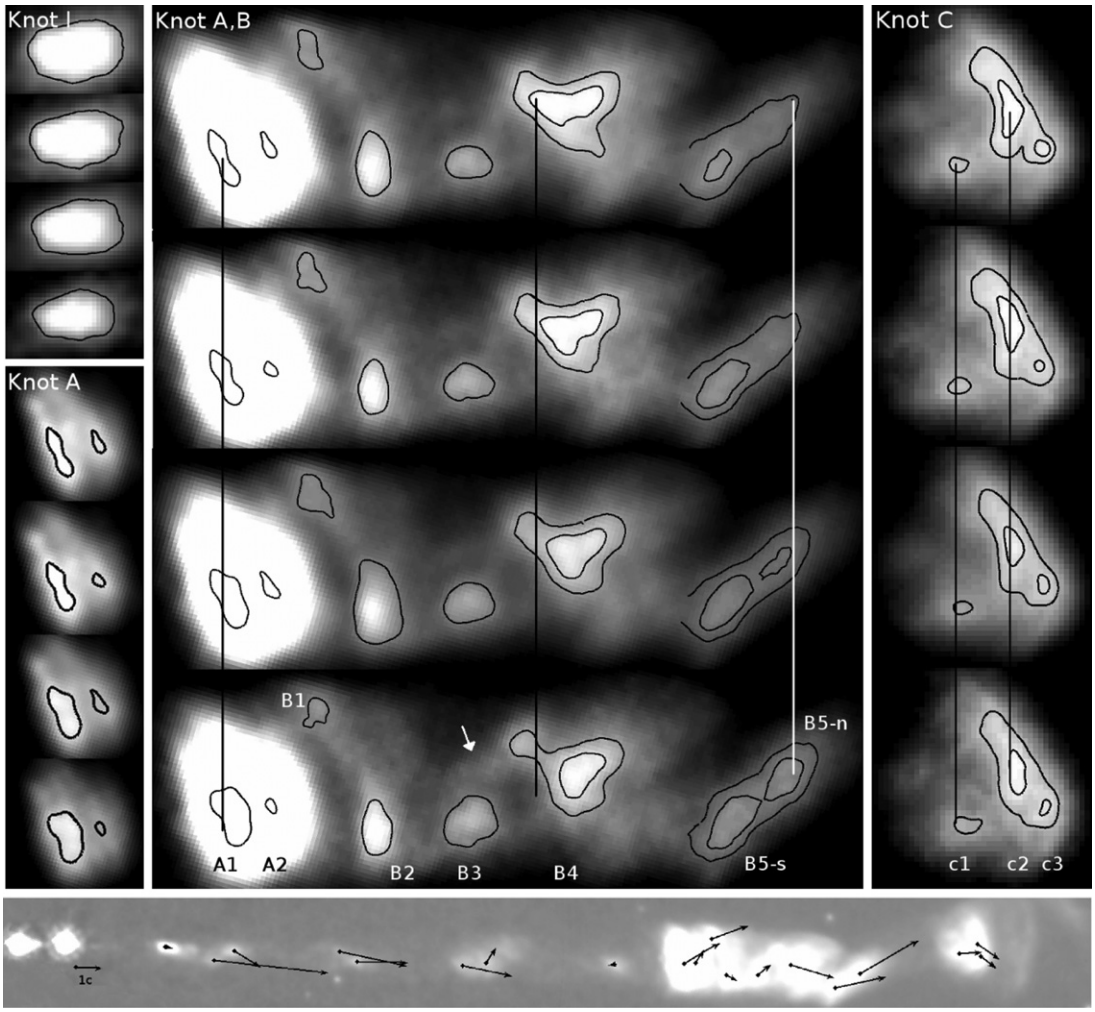

Figure 3. Upper left: knot I appears to fade and move backward along the jet at $0.23 \pm 0.12c$. Lower left: knot A is shown with a stretch to emphasize the fading of the knot over time. Middle panel: the knot A/B complex shows remarkable variability, with both sub-relativistic and superluminal apparent motions. The white arrow is pointing to a "bar" which appears in the last epoch. Right panel: knot C shows speeds on the order of 0.4–0.9c. Bottom panel: a depiction of velocities as vectors from their positions along the jet.

(Animations of this figure are available in the online journal.)

slope of zero, with typical errors on the order of 0.003 pixels yr^{-1} or 0.02c.

3. RESULTS

Starting from the core, the first well-detected features in our data set include a small narrow extension from the core (out to ∼0.″5) probably corresponding to knot L seen in VLBI images, as well as the famous variable feature, HST-1. Both the core and HST-1 are highly variable in flux and frequently saturated in our images. Because special care must be taken with saturated images, an analysis of the inner region of the M87 jet up to and including HST-1 will be addressed in a follow-up to this Letter. For all the knots described below, the WFPC2 image stacks (galaxy subtracted) described above are shown in Figures 1 and 3.

3.1. The Inner Jet: Knots D, E, F, and I

Knot D is the most consistently bright feature after the knot A/B/C complex, and significant proper motions were measured in both previous studies.[5] As suggested by the contours overlaid on Figure 1, D-Middle is one of the fastest components with a speed of $4.27 \pm 0.30c$ along the jet, while the brighter D-West shows evidence of *deceleration* radially, slowing to a near stop by the final epoch in 2008, while maintaining one of the largest transverse speeds of $-0.59 \pm 0.05c$ (see Figure 2). These measurements are consistent with the results of B99 ($5.26 \pm 0.92c$ and $2.77 \pm 0.98c$ for D-Middle and D-West, respectively), where we compare with our estimated velocity of D-West in 1996 of $2.73 \pm 0.40c$ from the quadratic fit.

Previous results on knot D-East have been conflicting: B95 found that it moved *inward* along the jet at $0.23 \pm 0.12c$ (possibly consistent with being stationary), while B99 found a large outward apparent velocity of $3.12 \pm 0.29c$; our result of 0.28 ± 0.05 is more in line with B95. It is possible that there is a stationary feature at D-East, through which components emerge (analogous to what is seen in HST-1). In that case, the higher-resolution Faint Object Camera was perhaps tracking

[5] It is important to note that B95 used data from 1985 through 1995, and so directly precedes the epoch of our data set, while B99 overlaps with only the early part of it, spanning 1995–1998. All β_{app} (including previous work) were computed with the conversion factor $0.264c$ yr mas^{-1}.

an emerging bright component, while over longer periods the global feature at D-East is stationary.

As shown in the central lower panel of Figure 1, the main knot structure of knot E (E-West) is complex, with a moderately superluminal speed of $1.91 \pm 0.14c$, about half of that found in B99 ($4.07 \pm 0.85c$). In addition to the 50% intensity contrast contour line shown, a lower-intensity contour at 30% has been drawn around this area to illustrate the morphological changes of this feature over time. To the west there appears a bright extension in the 1995 epoch which advances westward faster than the brightest part, and rapidly fades in the later epochs. Interestingly, a new component appears to the east in 2008, suggesting again the possibility of a favored location or stationary feature, which should be checked with future observations.

Like knot E, the next feature in the jet, knot F, is diffuse, faint, and apparently complex. We track two broad features, F-East and F-Middle, as shown in the lower right of Figure 1. As B99 were unable to measure proper motions for anything beyond knot E, the only previous measurement gives $0.90 \pm 0.23c$ in B95, for the entire diffuse feature seen in the radio. This is slightly faster than the value we measure for the most prominent component F-Middle ($0.36 \pm 0.14c$); however, the epochs of observation are not contemporaneous and slight deceleration is possible.

Finally, knot I has a slight negative velocity along the jet axis, of $-0.23 \pm 0.12c$. The knot clearly fades steadily with time, as shown in the upper left of Figure 3. This knot is the clearest case of a possible stationary feature in the jet outside of the upstream component HST-1d which has been extensively observed with VLBI ($\beta_{\rm app} < 0.25c$; Cheung et al. 2007).

3.2. The Outer Jet: Knots A, B, and C

The outer part of the jet looks very different from the evenly spaced knots discussed previously. Knot A is the brightest feature in the entire jet, excepting HST-1 during its remarkable flare of 2002–2008 (Harris et al. 2006). It has been suggested that knot A is an oblique shock which precipitates the breakup of the orderly structure of the jet, thus resulting in the complex knot B region downstream, and the final knot C feature which is considerably off the main jet axis (Bicknell & Begelman 1996). Within the bright but extended knot A, we track two features which appear on top of this more diffuse emission (see Figure 3). For A1, we find a relativistic velocity of $1.32 \pm 0.12c$; however, it is not clear that this feature is really a single component, as the western side of it appears to move slowly, if at all. For A2, we measure a much slower radial velocity of $0.31 \pm 0.06c$, consistent with the previous results of 0.4–0.6c from B95.

Qualitatively, the A/B complex is surprisingly "active" with new features brightening up and moving with high speeds relative to other nearby components. A good example is pointed out by the arrow in the last epoch of the central panel in Figure 3, where a "bar" has formed between B3 and B4. At the same time, within region B4 a separation is taking place, leaving a small knot behind to the northeast. While B4 is probably a complex of at least two to three "subknots," we used the inner contour (at 80% median flux), giving us an apparent speed of $1.66 \pm 0.11c$ along the jet direction. B1, B2, and B3 as well as the final knot C show significant apparent velocities in both directions, on the order of 0.5–1.5c.

The final terminus of knot B is particularly interesting, as a new distinct component (which we have labeled B5-n) appears in the northern half in the 2001 epoch. Using data from 2001–2008 only (the time when this component was detected), we measure an apparent velocity of $2.16 \pm 0.35c$ along the jet direction and $1.30 \pm 0.31c$ in the transverse direction. Qualitatively, the northern end of B5 seems to continuously brighten while the whole feature stretches up toward the northwest. In knot B, generally there is a repeating motif of two bright regions connected by a fainter "bar"; this is apparent between knots B1 and B2, between B3 and the remnant of B4, and the two halves of B5.

The most striking finding of the outer jet component velocities is depicted in the lower panel of Figure 3, where the velocity vectors are plotted from the center of each knot. There is a conspicuous "tip-to-tail" alignment of almost all the vectors within the outer knot A/B/C complex, strongly suggestive of a flattened view of a helical motion which might result in such a "zig-zag" pattern, though this should be checked with theoretical modeling.

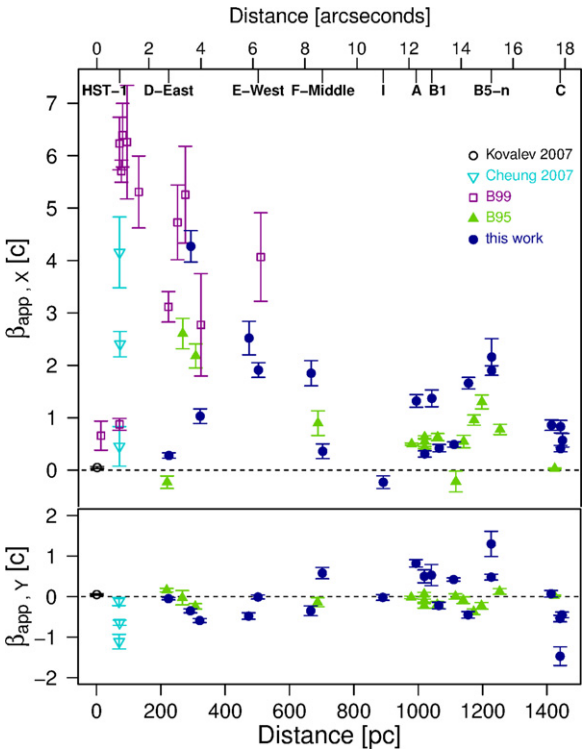

Figure 4. Velocities along the jet (upper panel) and transverse to the jet (lower panel) as a function of distance from the core. Previous measurements shown for comparison taken from B95, B99, Cheung et al. (2007), and Kovalev et al. (2007).

(A color version of this figure is available in the online journal.)

4. DISCUSSION AND CONCLUSIONS

We have presented new proper motion measurements for the knots in the M87 optical jet, reaching accuracies better than 0.1c. The speeds are largely in agreement with previous results where they exist (see Figure 4); some discrepancies are likely due to the higher resolution in the optical allowing us to track more compact features than those measured in the radio, or changes such as the observed deceleration of knot D-West. We also find evidence of stationary features in knots D-East, I, and possibly E (if the new extensions in 2008 is a recurrence at a preferred location), which should be checked with future observations.

Both D-Middle and the small component extending from D-East (labeled with an arrow in Figure 1) appear to steadily drop in intensity over the 13 yr of observation, a very similar behavior to the western components of knot HST-1 (e.g., B99), and both HST-1 and knot D are dominated by a transverse magnetic field as noted by Perlman et al. (1999), which suggests a shock at these locations. It has been suggested that at the eastern edge of HST-1 there is a recollimation shock (Stawarz et al. 2006; Cheung et al. 2007; see also Asada & Nakamura 2012), but the appearance of very different speeds all along the jet might also be consistent with pairs of forward/reverse fast-mode MHD shocks in a strongly magnetized relativistic flow (Nakamura et al. 2010).

In the outer jet (from knot A), we find apparent velocities that are still superluminal and velocity vectors that appear to line up into a helical/side-to-side pattern. However, it is not clear that the measured speeds can be identified with discrete moving components. It is possible that if the jet of M87 has a helical structure which is broken up at knot A, we are seeing the "unwinding" of the coil in knot B. Thus the appearance of the bar noted with an arrow in 2008 could be the result of a change in geometry as the coil of the jet unwinds, bringing a length into our line of sight. Sideways oscillation of components B1–B5 may presumably follow a helical path of underlying magnetic fluxes (Owen et al. 1989; Perlman et al. 1999) in three dimensions. Thus, the knot A/B/C complex could be seen as a consequence of the interplay between the slow-mode MHD shocks and growing helical kink instability (Nakamura & Meier 2004).

Support for this work was provided by NASA through a grant for archival program 12635 from the Space Telescope Science Institute (STScI), which is operated by the Association of Universities for Research in Astronomy (AURA), Inc., under NASA contract NAS5-26555. This project is part of the HSTPROMO collaboration (www.stsci.edu/∼marel/hstpromo.html), a set of HST projects aimed at improving our dynamical understanding of stars, clusters, and galaxies in the nearby universe through measurement and interpretation of proper motions.

Facility: HST (WFPC2, ACS).

REFERENCES

Anderson, J., & van der Marel, R. P. 2010, ApJ, 710, 1032
Asada, K., & Nakamura, M. 2012, ApJL, 745, L28
Bicknell, G. V., & Begelman, M. C. 1996, ApJ, 467, 597
Biretta, J. A., Sparks, W. B., & Macchetto, F. 1999, ApJ, 520, 621
Biretta, J. A., Zhou, F., & Owen, F. N. 1995, ApJ, 447, 582
Blakeslee, J. P., Jordán, A., Mei, S., et al. 2009, ApJ, 694, 556
Cheung, C. C., Harris, D. E., & Stawarz, Ł. 2007, ApJL, 663, L65
Curtis, H. D. 1918, PLicO, 13, 9
Harris, D. E., Cheung, C. C., Biretta, J. A., et al. 2006, ApJ, 640, 211
Junor, W., & Biretta, J. A. 1995, AJ, 109, 500
Kovalev, Y. Y., Lister, M. L., Homan, D. C., & Kellermann, K. I. 2007, ApJL, 668, L27
Marshall, H. L., Miller, B. P., Davis, D. S., et al. 2002, ApJ, 564, 683
Nakamura, M., Garofalo, D., & Meier, D. L. 2010, ApJ, 721, 1783
Nakamura, M., & Meier, D. L. 2004, ApJ, 617, 123
Owen, F. N., Hardee, P. E., & Cornwell, T. J. 1989, ApJ, 340, 698
Perlman, E. S., Biretta, J. A., Zhou, F., Sparks, W. B., & Macchetto, F. D. 1999, AJ, 117, 2185
Perlman, E. S., Sparks, W. B., Radomski, J., et al. 2001, ApJL, 561, L51
Perlman, E. S., & Wilson, A. S. 2005, ApJ, 627, 140
Reid, M. J., Biretta, J. A., Junor, W., Muxlow, T. W. B., & Spencer, R. E. 1989, ApJ, 336, 112
Sohn, S. T., Anderson, J., & van der Marel, R. P. 2012, ApJ, 753, 7
Sparks, W. B., Biretta, J. A., & Macchetto, F. 1996, ApJ, 473, 254
Stawarz, Ł., Aharonian, F., Kataoka, J., et al. 2006, MNRAS, 370, 981
Walker, R. C., Ly, C., Junor, W., & Hardee, P. J. 2008, JPhCS, 131, 012053